This article has been accepted for publication in a future issue of this journal, but has not been fully edited. Content may change prior to final publication. Citation information: DOI 10.1109/TMECH.2020.3029579, IEEE/ASME Transactions on Mechatronics

Shock Isolation Capability of an Electromagnetic Variable Stiffness Isolator with Bidirectional Stiffness Regulation

Jinglei Zhao#, Yi Sun#, *Member, IEEE,* Jiheng Ding, Yu Sun, *Fellow, IEEE,* Min Wang, Shujin Yuan, Huayan Pu*, Jun Luo, Zhijiang Xie, Yi Qin, Jing Wei, Shaorong Xie, and Yan Peng.

***Abstract*—This study presents a novel electromagnetic variable stiffness isolator that achieves bidirectional stiffness regulation, which means that the isolator experiences a reduced stiffness when the applied current is positive and an increased stiffness when the opposite current is applied. In addition, the stiffness variations are equal for two currents with the same magnitude but opposite polarities. The proposed isolator can not only ensure the vibration isolation performance in working frequency zone that is relatively far from the natural frequency, but also can realize high-damping-like effect for shock response attenuation, without introducing any additional damping components that may complicate the system. The bidirectional stiffness regulation was realized by combining mechanical springs with hybrid magnets (permanent magnets and coil windings). Variation in the overall stiffness of the proposed isolator occurred when the current was continuously adjusted. A prototype of the isolator was designed, fabricated and then tested with a round displacement step shock at the base. The theoretical analysis revealed that this device could be utilized as an active vibration isolator through certain control strategies. The experimental results proved the effectiveness of the proposed mechanism in shock isolation and revealed that it outperforms the conventional isolator in suppressing the residual vibration.**

***Index Terms*—Shock isolation, variable stiffness, electromagnetic mechanism**

I. Introduction

Shock and vibration widely exist in various mechanical systems, and it is one of the main factors that damages machines and sensors [1–4]. Typically, shock isolation can be divided into two categories: isolation of the transient response and suppression of the residual vibration when the shock ends. The purpose of the former category is to reduce the overshoot of the response when the equipment is subjected to a shock input, while the later category focuses on how to ensure that the residual vibration decays rapidly so that the system restore its steady state quickly [5–7]. A common practice to deal with the shock input is to introduce additional damper into the isolation system [8]. But in some application scenarios, when the isolated equipment requires the isolator to have a natural frequency that is far from the working frequency (excitation frequency), the damping and stiffness of the isolation system should be as low as possible to ensure a better isolation performance within the working frequency zone. However, there is an inherent shortcoming for such a low-damping system, namely, the poor performance in attenuating the response for shock input. This is because the response after shock input can be essentially regarded as free vibration, which implies that the isolator is working at the natural frequency. For such a system that is working near the natural frequency, larger damping coefficient is more preferable because it can attenuate the shock response rapidly. In order to cope with this contradiction, an approach based on variable stiffness has been proposed. This approach can not only ensure the vibration isolation performance in working frequency zone that is far from the natural frequency, but also can realize high-damping-like effect for shock response attenuation, without introducing additional damping component/system which may complicate the entire system.

As a result, isolation systems with high-static-low-dynamic stiffness (HSLDS) [9–14] or nonlinear negative stiffness [15–18] have become a promising choice for shock isolation, and there has been several pioneering works about the potential of the variable stiffness (VS) systems in isolating shock input [19, 20]. The basic idea is to switch the stiffness from one value to another value in a periodic manner to gradually dissipate system energy [21], and the larger the range of stiffness regulation, the quicker the dissipation of energy. Conventional VS isolators or strategies usually concentrate on the VS effect in terms of reducing the overall stiffness by adding a positive stiffness (PS) in series or connecting a parallel negative stiffness (NS). For example, Onoda *et al.* [22, 23] presented theory of a serial-stiffness-switch system. In the system, when one spring is closed, the system shows a large stiffness, and vice versa; Ledezma *et al.* [24–26] combined a novel switchable electromagnetic stiffness mechanism with nylon wires to realize HSLDS; Chen *et al.* [27] originally proposed a stiffness switching strategy that switched the

J. Zhao, J. Luo, Z. Xie, Y. Qin, J. Wei are with the State Key Laboratory of Mechanical Transmissions, Chongqing University, Chongqing, China.

Y. Sun, J. Ding, M. Wang, S. Yuan, H. Pu, S. Xie and Y. Peng are with the School of Mechatronics Engineering and Automation, Shanghai University, Shanghai, China.

Y. Sun is with the Department of Mechanical and Industrial Engineering, University of Toronto, Toronto, M5S 3G8, Canada.

#These authors contributed equally. This work was supported by the National Natural Science Foundation of China under Grants 51575329,61773254,61625304 and 61873157; in part by Shanghai Rising-Star Program under Grants 17QA1401500; in part by Science and Technology Commission of Shanghai under Grants 16441909400 and 17DZ1205000.

*Corresponding author: H. Pu (email: phygood_2001@shu.edu.cn).

This article has been accepted for publication in a future issue of this journal, but has not been fully edited. Content may change prior to final publication. Citation information: DOI 10.1109/TMECH.2020.3029579, IEEE/ASME Transactions on Mechatronics

stiffness between a high-state and a low-state periodically. The essence of both these studies is to adopt one stiffness for a particular motion phase and then connect another stiffness component in series (Onoda *et al.*) or superpose a negative stiffness (NS) (Ledzma *et al.*) if the phase changes.

In this work, however, a novel EVS isolator that can achieve *bidirectional regulation* of the stiffness is designed by combining two mechanical springs with a nesting-type hybrid magnetic mechanism. This configuration allows the overall stiffness of the EVS isolator to be increased and decreased by regulating the magnitude and polarity of the current. Specifically, if a conventional VS isolator is utilized as a shock isolator, it can achieve a stiffness scope of $[k - k_{aux}, k]$, where $k_{aux} \geq 0$ is the auxiliary stiffness generated by the VS/EVS mechanism. However, the proposed design with bidirectional stiffness regulation can extend this strategy through achieving a larger stiffness range of $[k - k_{aux}, k + k_{aux}]$.

In our previous work [28], we proposed a tunable stiffness isolator with compact structure and validated its effectiveness in vibration isolation. Compared with the previous work, the originality of this paper is as follows:

1) A new EVS isolator is designed and fabricated, and its advantage of bidirectional stiffness regulation could be applied to improve the shock isolation logic compared with the conventional isolators.
2) The round displacement step (RDS) shock input is reproduced in the laboratory, and the response is studied experimentally. To a certain extent, the experimental results in this paper overcomes the shortage of the related research in terms of lack of experimental data.
3) Both the effects of the conventional logic and the extended strategy for residual vibration suppression are evaluated through the proposed prototype. The results show that the extended strategy outperforms the conventional strategy by a reduction in the settling time of as much as 33.7%.

II. System Description

A. Prototype design

To design an EVS isolator with bidirectional stiffness regulation, a compact electromagnetic mechanism that can produce a negative or positive interaction force is designed first. This novel electromagnetic mechanism consists of two mechanical springs and a hybrid magnet mechanism comprising four permanent magnets (PMs) and four coil windings (CWs). Fig. 1 shows the assembly of the EVS isolator and the controllable electromagnetic mechanism. All four PMs and the CWs are placed consecutively in the axial direction. Then, the PMs are nested into the CWs, which are hollow inside. Four shaft collars, which are labeled as C1 to C4, are fastened on the shaft. C2 and C3 are utilized to fix the PMs; The pre-stressed mechanical spring is installed between the linear bushing and the shaft collar (C1 or C4). If the shaft moves relative to the frame and the CWs are energized, an electromagnetic force generated by the hybrid magnet mechanism and a restoring force provided by the mechanical springs will exert on the shaft simultaneously. These two forces may cancel out or superimpose on each other. All the structural parameters are listed in Table I.

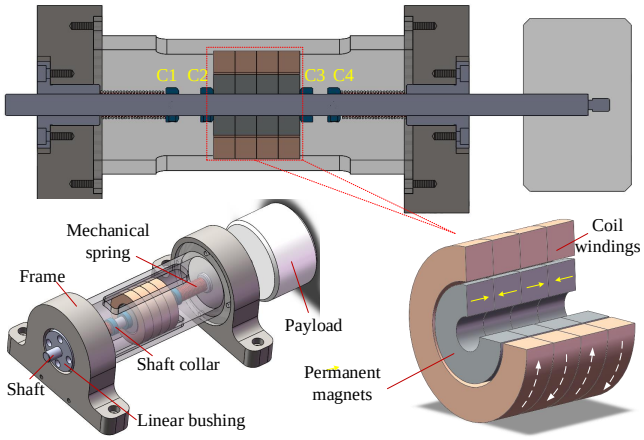

Fig. 1. Schematic diagram of the EVS isolator. The solid arrows and dashed arrows correspond to the magnetizing and current directions, respectively.

TABLE I
STRUCTURAL PARAMETERS AND VARIABLES OF THE SYSTEM.

Para.	Value	unit	Definition
Structural Parameters			
m	2.818	kg	Mass of the payload.
c	0.037	Ns/mm	Equivalent damping.
k_s	4.086	N/mm	Stiffness of the mechanical spring.
ω_n	38	rad/s	Natural frequency of the linear system.
T	0.165	s	Natural period of the linear system.
R	4.05	Ω	Resistance of single coil winding.
Variables			
ξ	–	–	Equivalent damping ratio.
p_i *	–	–	Fitting parameters.
K_1	–	–	Dimensionless linear stiffness.
K_j *	–	–	Dimensionless nonlinear stiffness.
I	–	A	Excited current of coils.
Y	–	mm	Shock amplitude.
$\hat{Y}$	–	–	Dimensionless shock amplitude.
y, x	–	mm	Displacement of the base/payload.
u	–	mm	Relative displacement of the payload.
$\hat{y}$, $\hat{x}$	–	–	Dimensionless base/mass displacement.
$\hat{u}$	–	–	Dimensionless relative displacement of the payload
β	–	–	Severity parameter.
t, τ	–	s, –	Time/Dimensionless time.
t_r	–	s	Rise time.

* i = 1,3,5,7,9, j = 3,5,7,9.

B. Mechanism of the bidirectional stiffness regulation

Because of the axial symmetry of the proposed EVS isolator, only the axial electromagnetic force is exerted on the PMs. When the CWs are not energized or the PMs are in their equilibrium locus, the force exerted on the PMs by the CWs is zero. In this case, the stiffness of the entire system equals the stiffness of the mechanical spring. However, the steady state will be broken by the relative motion between the PMs and the CWs if the CWs are current-carrying. Specifically, an auxiliary electromagnetic force will be exerted on the PMs. The magnitude and direction of this electromagnetic force depend on the magnitude and polarity of the current. If the electromagnetic force and the restoring force of the spring are

This article has been accepted for publication in a future issue of this journal, but has not been fully edited. Content may change prior to final publication. Citation information: DOI 10.1109/TMECH.2020.3029579, IEEE/ASME Transactions on Mechatronics

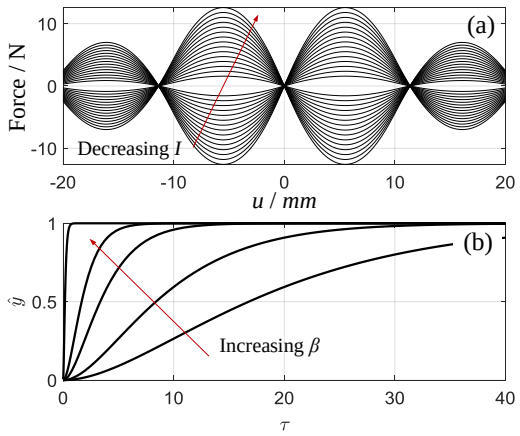

Fig. 2. Simulation curves. (a) Electromagnetic forces for various currents from 1.2 A to -1.2 A with a step of 0.1 A. (b) RSD shock inputs for various severity parameters β.

opposite in direction, the electromagnetic force will counteract the restoring force provided by the mechanical springs. As a result, the resultant force exerted on the PMs reduces, which means that the overall stiffness of the EVS isolator decreases as well. On the contrary, if the electromagnetic force and the restoring force are in same direction, the overall stiffness will increase accordingly.

III. Modeling the EVS Isolator

A. Modeling the electromagnetic stiffness

The overall stiffness of the isolator is dependant on the stiffness of the mechanical spring and the electromagnetic mechanism. The electromagnetic stiffness/force can be calculated by the so called $filament\ method$ [29, 30]. The principal of this method is to transfer the PM/CW into discrete current-carrying filaments equivalently, then calculate the interaction force between each pair of coils, and finally sum the interaction forces through a superposition. A detailed calculation procedure has been given in previous studies [10, 31] and hence is omitted here. The total electromagnetic force f^* of the four-magnet-four-winding configuration can be calculated using

$$f^* = \sum_{a=1}^{4}\sum_{b=1}^{4} F_{C_a M_b} \tag{1}$$

where $F_{C_a M_b}$ (a, b = 1,2,3,4) denotes the electromagnetic force between the a-th PM and the b-th CW. With this computation method, the electromagnetic force for the proposed system can be calculated and is shown in Fig. 2a for various currents. However, the expression obtained from Eq. 1 is complicated because it contains elliptic integral and summation notation [28]. Thus, in order to clearly establish motion equations and explain the EVS mechanism, we simplify the expressions of the electromagnetic force by fitting them to a ninth order polynomial of the form

$$f^* = \sum_i p_i u^i, (i = 1, 3, 5, 7, 9) \tag{2}$$

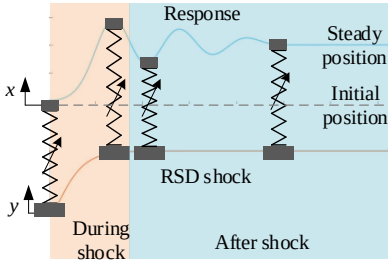

Fig. 3. Schematic of the EVS isolator subjected to a shock.

where p_is are fitting parameters computed according to the method of least square fitting, and the fitting order is set to be ninth order. Ten coefficients, which represent the coefficients of the polynomial, are obtained. The coefficients for even order terms are neglected because they are relatively small compared with odd ones. The fitting results are listed in Table II. Based on the fitting results, the maximum fitting error is 6 %, which verifies the reliability and practicality of the fitting.

B. Expression of the RSD shock input

A round displacement step (RDS) shock input, which is commonly selected as a base shock [32], is considered in this paper. It can be expressed as

$$y = Y\left[1 - (1 + \beta\omega_n t)\, e^{-\beta\omega_n t}\right] \tag{3}$$

where Y denotes the actual amplitude of the RDS shock input (namely, the maximum displacement of the base) and $\omega_n = \sqrt{k_s/m}$ is the natural frequency of the system when there is no current in the CWs. In the following sections, for describing the relationship between the shock amplitude and the characteristic of the nonlinear system more clearly, the shock amplitude is non-dimensionalized as $\hat{Y} = Y/L$, where L = 5 mm is the negative stiffness range of the system.

Following Tang $et\ al.$ [6], β is defined as the severity parameter that indicates the steepness of the RDS shock, which equals the ratio of the period of the natural vibration of the linear isolation system T to twice the rise time t_r, namely, $\beta = T/2t_r$. The rise time is the time when the displacement reaches 82% of its steady-state value. Shock inputs with different β values are shown in Fig. 2b, from which one can see that the steepness of the curve becomes severe with an increase in β. Eq. 3 can also be expressed in dimensionless form as

$$\hat{y} = 1 - (1 + \beta\tau)\, e^{-\beta\tau} \tag{4}$$

where $\hat{y} = y/Y$ is the dimensionless base displacement and $\tau = \omega_n t$ is the dimensionless time [5, 6, 20]. By differentiating Eq. 4 with respect to the dimensionless time τ, the dimensionless acceleration of the RDS can be derived as

$$\hat{y}'' = -\beta^2 e^{-\beta\tau}\,(\beta\tau - 1) \tag{5}$$

C. Motion equation with the RDS shock input

Fig. 3 illustrates the RDS shock applied at the base and the response of the payload. It is noteworthy that the response

This article has been accepted for publication in a future issue of this journal, but has not been fully edited. Content may change prior to final publication. Citation information: DOI 10.1109/TMECH.2020.3029579, IEEE/ASME Transactions on Mechatronics

TABLE II
FITTING PARAMETERS FOR VARIOUS CURRENTS

I/A	p_1	p_1	p_1	p_1	p_1
0	0	0	0	0	0
±0.4	±1857.66	∓2.62e+7	±1.19e+11	∓2.37e+14	±1.81e+17
±0.8	±3715.31	∓5.24e+7	±2.39e+11	∓4.75e+14	±3.61e+17

of the payload to a RDS shock input is a two-stage process, namely, during and after the shock. Therefore, the motion equation can be expressed by a piecewise function by assuming that: during the shock, the acceleration of the base is $\ddot{y}$ ($\ddot{y} \neq 0$); after the shock (during the residual vibration), the acceleration of the base is zero ($\ddot{y}$ = 0, $i.e.$, there is no input to the isolator). The equation of motion for an isolated payload with respect to the relative displacement (deformation of the mechanical springs) u = x - y is given by

$$m\ddot{u} + c\dot{u} + k_s u - f^* = -m\ddot{y} \tag{6}$$

where the dots $\cdot$ denote the derivatives with respect to time t, $k_s > 0$ denotes the stiffness coefficient of the spring, and $c > 0$ denotes the equivalent damping coefficient. Substituting Eq. 2 into Eq. 6, then collecting the terms that involve u, the following equation can be obtained

$$m\ddot{u} + c\dot{u} + (k_s - p_1)\, u - \sum_{j=3,5,7,9} p_j u^j = -m\ddot{y} \tag{7}$$

In the above equation, u can be nondimensionalized as $\hat{u} = u/Y$; in addition, since $\dot{u} = Y\omega_n \hat{u}'$ and $\ddot{u} = Y\omega_n^2 \hat{u}''$ (the primes $'$ denote the derivatives with respect to the dimensionless time τ), one can obtain the dimensionless format of Eq. 7 as

$$Y\omega_n^2 \hat{u}'' + \frac{c}{m} Y\omega_n \hat{u}' + \frac{k_s - p_1}{m} Y\hat{u} - \sum_{j=3,5,7,9} \frac{p_j}{m} Y^j \hat{u}^j = -\ddot{y} \tag{8}$$

Eq. 8 can be further simplified as

$$\hat{u}'' + 2\xi\hat{u}' + K_1\hat{u} + \sum_{j=3,5,7,9} K_j \hat{u}^j = \hat{F}(\beta) \tag{9}$$

where

$$\xi = \frac{c}{2m\omega_n}, K_1 = \frac{k_s - p_1}{k_s}, K_j = -\frac{p_j Y^{j-1}}{k_s}, \hat{u} = \frac{u}{Y}$$

$$\hat{F}(\beta) = \begin{cases} -\frac{1}{\omega_n^2}\frac{\ddot{y}}{Y} = -\hat{y}'' & , \ during\ the\ shock \\ 0 & , \ after\ the\ shock \end{cases}$$

D. Evaluation of the performance for the proposed system

Three indices are utilized to evaluate the shock isolation performance, and one is adopted to evaluate the residual vibration suppression performance of the system, they can be expressed as:

- Maximum absolute acceleration ratio (MAAR) = $|\hat{x}''|_{\max}/|\hat{y}''|_{\max}$.
- Maximum absolute displacement ratio (MADR) = $|\hat{x}|_{\max}/\hat{y}_{\max}$.
- Maximum relative displacement ratio (MRDR) = $|\hat{x} - \hat{y}|_{\max}/\hat{y}_{\max}$.
- Settling time τ_s, the time required for the response curve to reach and stay within a range of 5% of the steady position.

The MAAR and MADR indicate the maximum shock acceleration and displacement transmissibility, respectively. To protect equipment that is sensitive to acceleration/displacement, the MAAR/MADR should be as small as possible. The MRDR is also of great importance because it indicates the deformation of the isolation system. A larger deformation may cause failure of the vibration isolator and even result in a collision between the base and the isolated equipment. In order to discuss the effect more clearly, the MAAR is presented in dB, namely, $20 \cdot \lg(|\hat{x}''|_{\max}/|\hat{y}''|_{\max})$. When the shock ends, the settling time τ_s is introduced to indicate the mean time between the beginning of the shock and the payload returning to its steady position (5% error band). From the perspective of shock/vibration suppression, a smaller τ_s is more preferable.

IV. NUMERICAL ANALYSIS

To further explain how the proposed EVS isolator works, we discuss its application in shock isolation and residual vibration suppression through numerical simulation in this section. The response of the system subjected to an RDS shock input is obtained by solving Eq. 9 numerically utilizing the ODE45 algorithm in MATLAB. The magnitude/polarity of the current I, the amplitude $\hat{Y}$ and the severity parameter β of the RDS shock are key factors that influence the nonlinearity of the system and hence the shock isolation performance. It is noteworthy that the direction of the current varies such that the generated electromagnetic force f^*, the linear stiffness coefficient K_1, and the nonlinear stiffness coefficients K_j (j = 3,5,7,9) can be positive or negative. All the corresponding dimensionless stiffness coefficients (both linear and nonlinear) are calculated through p_j listed in Table II. It needs to be noted: (1) I = 0 A corresponds to a linear/passive system without VS; (2) with increases in the current magnitude I and shock amplitude $\hat{Y}$, the nonlinear coefficients K_j (j = 3,5,7,9) increase. Namely, the effect of the current I on the nonlinearity of the system has the same trend with that of the amplitude $\hat{Y}$ of the shock input.

The feature of bidirectional stiffness regulation allows the EVS isolator to regulate its stiffness characteristics and hence influence the shock isolation performance such as the MAAR, MADR and MRDR, the simulated results will be illustrated in the next section, along with the experimental verifications. In this section we will concentrate on another typical application of the bidirectional stiffness regulation, namely, suppressing the residual vibration when the shock ends. Consider a linear single degree of freedom (SDOF) mass-spring-damper system. The regulation strategy for residual vibration suppression can be stated as: If the payload moves away from its steady position ($u\dot{u} > 0$, pink area in Fig. 4a), the overall stiffness of the system remains high, $i.e.$, k_{high}. The maximum potential energy V_{high} is

This article has been accepted for publication in a future issue of this journal, but has not been fully edited. Content may change prior to final publication. Citation information: DOI 10.1109/TMECH.2020.3029579, IEEE/ASME Transactions on Mechatronics

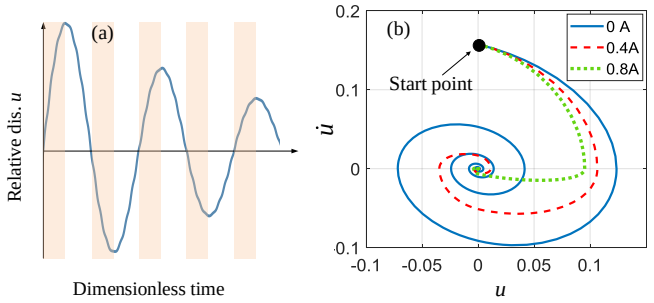

Fig. 4. The schematics of the bidirectional stiffness regulation. (a) regulation strategy; (b) phase plane plot.

$$V_{high} = \frac{1}{2} k_{high} u_{max}^2 \tag{10}$$

where u_{max} is the maximum deformation of the EVS mechanism. Then, the overall stiffness suddenly switches to a lower value k_{low} until the payload reaches the steady position ($u\dot{u} > 0$, blank area in Fig. 4a). The maximum potential energy V_{low} at u_{max} in this situation is

$$V_{low} = \frac{1}{2} k_{low} u_{max}^2 \tag{11}$$

Finally, the loss in the potential energy V_{loss} can expressed as

$$V_{loss} = V_{high} - V_{low} = \frac{1}{2} \Delta k u_{max}^2 \tag{12}$$

where $\Delta k = k_{high} - k_{low}$ ($k_{high} \geq k_{low}$) implies the range of the stiffness regulation. During an oscillating cycle, a greater Δk may result in more loss in the potential energy and hence a larger decrease in the kinematic energy. In other words, the greater the decrease in kinematic energy, the quicker the payload converges to its steady position. More details about the mechanism of the energy dissipation could be found in [21]. Thus, generating a large Δk is the key to improving the performance of residual vibration suppression.

As mentioned above, one distinctive highlight of this paper is that the capability of bidirectional stiffness regulation enables the proposed EVS isolator to increase and decrease its overall stiffness, resulting in a greater Δk. Based on this feature, an extended strategy (with respect to the conventional ones[22–25]) is introduced in this section. The principal for these two strategies is listed in Table III. Basically, the conventional strategy can achieve a stiffness range of $[k_s - k_{aux}, k_s]$, which corresponds to $\Delta k = k_{aux}$. However, the extended strategy can realize a larger stiffness range of $[k_s - k_{aux}, k_s + k_{aux}]$ due to the bidirectional stiffness regulation through tuning the current I, corresponding to $\Delta k = 2k_{aux}$. In fact, Tran *et al.* [33] have already proposed a switchable stiffness system. This rather elegant design can be utilized to realize bidirectional stiffness regulation, but the effect is different from our proposed one. In his work, the absolute value of the auxiliary stiffness k_{aux} generated by equal but opposite currents was unequal. Specifically, the mechanism proposed by Tran *et al.* generates $-k_{big}$ if the current is $I = 0.8$ A and k_{small} if $I = -0.8$ A, where

TABLE III
THE PRINCIPAL FOR THE CONVENTIONAL STRATEGY AND THE EXTENDED STRATEGY

Type	Principal
Conventional	$k_e = \begin{cases} k & , u\dot{u} \geq 0 \\ k - k_{aux} & , u\dot{u} < 0 \end{cases}$
Extended	$k_e = \begin{cases} k + k_{aux} & , u\dot{u} \geq 0 \\ k - k_{aux} & , u\dot{u} < 0 \end{cases}$

$|k_{small}| < |k_{big}|$. Namely, it can realize a stiffness range of $[k - k_{big}, k + k_{small}]$ ($\Delta k = k_{big} + k_{small}$). To further broaden the stiffness range, a greater current is required to increase the value of k_{small}, which is dangerous and uneconomical due to the heat load by the CWs. This asymmetric feature limits its stiffness regulation range. For the proposed EVS isolator, however, the quantities of the generated stiffness are equal in magnitude for equal but opposite current I. Thus, in this sense, the proposed EVS isolator can still achieve a greater stiffness range of $[k - k_{big}, k + k_{big}]$ ($\Delta k = 2k_{big}$).

It is clear that a greater Δk may lead to a quicker convergence speed or a shorter settling time τ_s. The effect of the proposed extended strategy on the residual vibration suppression is simulated and analyzed in this section. In this simulation, currents of $I = 0$ A, ± 0.4 A and ± 0.8 A are applied to generate various Δk. The payload has an initial velocity of $\dot{u}(0) = 0.15$ and an initial displacement of $u(0) = 0$ at the start point. The simulation results of the phase plane plot is shown in Fig. 4b, from which one can see that the trajectory is getting closer to the original point every oscillation cycle. In addition, it can also be concluded that the convergence speed for $I = \pm 0.8$ A is the quickest due to the greatest Δk.

Please note that, in order to maintain the stability of the bidirectional stiffness regulation, the equivalent/overall stiffness should be greater than zero, because systems with purely negative stiffness would lose stability under a slight disturbance. For our proposed system, the positive definiteness of the equivalent stiffness is guaranteed by limiting the energizing current.

V. Experimental Verifications and Results

The experiments conducted below were designed with the following considerations: (a) to prove the effectiveness of the EVS isolator in shock isolation and residual vibration suppression; (b) to show the appreciable benefits of the proposed extended strategy which enables bidirectional stiffness regulation. Based on these considerations, we first verify the shock isolation strategy. Then, instead of discussing the extended residual vibration suppression strategy separately, we reasonably combine it with the shock isolation strategy from the perspective of practical application.

A. Experimental setups

Fig. 5 shows the detailed experimental setup for the shock test. The setup consists of an EVS isolator (see Fig. 1), a movable plate mounted on two guide tracks, an electromagnetic switch and a fixed plate. The EVS isolator is fixed to the movable plate, which can then move together on the

This article has been accepted for publication in a future issue of this journal, but has not been fully edited. Content may change prior to final publication. Citation information: DOI 10.1109/TMECH.2020.3029579, IEEE/ASME Transactions on Mechatronics

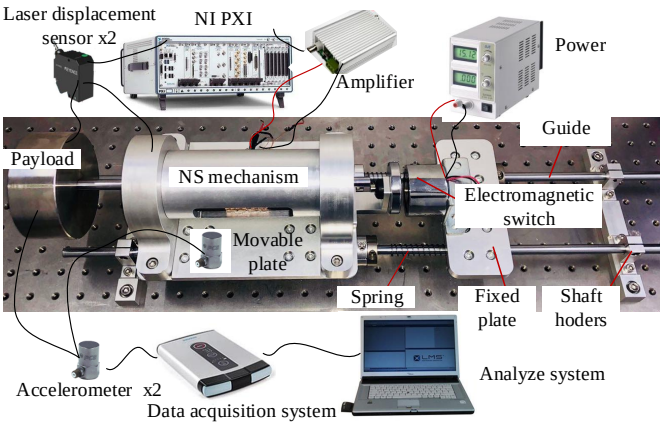

Fig. 5. Experimental setup.

guide tracks. The free end of the electromagnetic switch is attached to the movable plate, while the fixed end is mounted on the fixed plate. Two mechanical springs are nested on the guide tracks. An electromagnetic force will be generated when the switch is energized, and this force will compress the mechanical springs so that the fixed end and free end will be pulled together. When turning off the electromagnetic switch and releasing the free end after the experiment begins, the potential energy stored in the springs will be converted into kinetic energy of the movable plate. When the movable plate moves over a period of time, it collides with the shaft holders, which are fixed with the guide. We mimic the RDS shock as closely as possible in the way described above.

The acceleration signals for both of the isolated mass and the movable plate are measured by two PCB 356A17 accelerometers. The acceleration signals are collected by an LMS SCADAS XS device and are processed by LMS Test Lab software installed on a PC. The displacement signals are acquired by two Keyence LK G30A laser sensors and NI 6123 DAQ card. A FPA1000 direct current amplifier is utilized to energize the CWs. A mini DC power supply QJ3003A is adopted to supply current for driving the electromagnetic switch, which is also selected as the trigger signal for data acquisition.

B. Measurement of properties

The characteristics of the system, such as the natural frequency and damping coefficient, were measured experimentally through the transmissibility of the proposed system. The transmissibility can be calculated by the ratio of the acceleration signals for the payload to that of the movable plate in frequency domain. Transmissibility curves of the proposed system with different currents are shown in Fig. 6, through which one can see that the natural frequency of the proposed system depends on the magnitude and polarity of the current. It is noteworthy that a positive current means the EVS isolator will generate a negative EVS, which leads to a decrease in the overall stiffness of the system, and the converse is also true. Thus, with an increase in the current I (from negative to positive), the natural frequency of the proposed system shifts

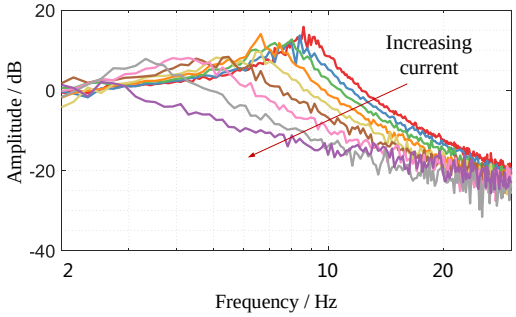

Fig. 6. Measured transmissibility curves for currents varying from - 0.8 A to 0.8 A with a step of 0.2 A.

TABLE IV
EQUIVALENT RESONANCE FREQUENCY MEASURED EXPERIMENTALLY

Current/A	-0.8	-0.6	-0.4	-0.2	0	0.2	0.4	0.6	0.8
Resonance/Hz	8.8	8.2	7.6	7.0	6.1	5.3	4.4	3.5	2.9

to the lower frequency band, specifically, from 8.8 Hz to 2.9 Hz, as listed in Table. IV.

For the proposed system, the damping coefficient c for passive/linear system is evaluated by the half-power bandwidth method and is calculated to be 0.037 Ns/mm (corresponding to a damping ratio ξ of 17.24%). Another interesting note is that the transmissibility peak values also decrease as the current increases. This is mainly because the equivalent damping ratio ξ increases with the decrease in the overall stiffness of the system. The response speed for the EVS isolator is also crucial for the performance, and it can be evaluated by measuring the time delay between the input signal and response of the CWs. For the proposed EVS isolator, the delay is about 11 ms, which can satisfy the engineering application requirement. Another characteristic of the proposed system is its power consumption, which can be calculated through the current and the resistance of the CWs. For the proposed system, the maximum power is about 10.37 W when current I = 0.8 A (room temperature).

C. Shock isolation through stiffness regulation

Shock isolation experiments are carried out with the experimental platform shown in Fig. 5. By restricting the movement of the movable plate before colliding with the shaft holders and adjusting the deformation of the springs, the platform can

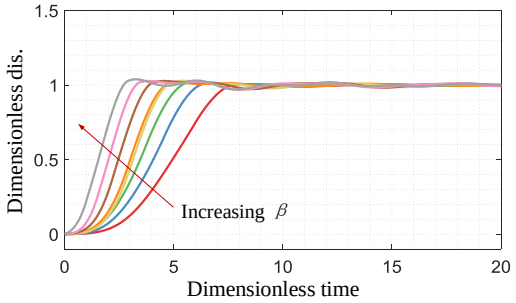

Fig. 7. RSD shock inputs measured by the displacement sensor for different severity parameters β.

This article has been accepted for publication in a future issue of this journal, but has not been fully edited. Content may change prior to final publication. Citation information: DOI 10.1109/TMECH.2020.3029579, IEEE/ASME Transactions on Mechatronics

TABLE V
CHARACTERISTICS OF THE EXPERIMENTAL RDS SHOCK INPUT

No.	1	2	3	4	5	6	7	8
Rise time/s	0.147	0.121	0.112	0.090	0.076	0.064	0.060	0.055
β	0.56	0.68	0.74	0.92	1.09	1.29	1.38	1.51

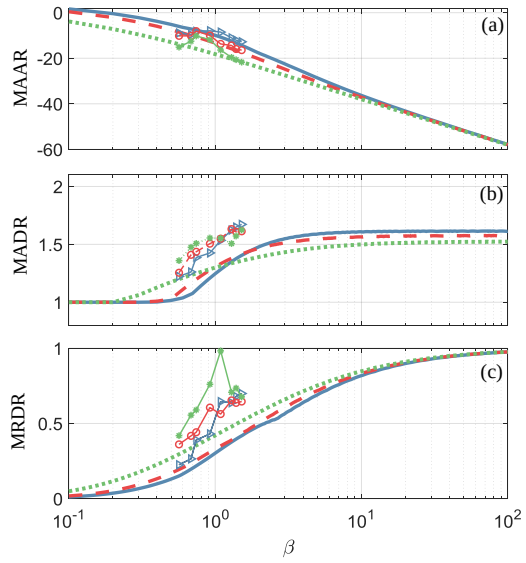

Fig. 8. Comparison of the experimental and analytical results. The curves with the asterisk (*) / circle (○) / triangle (△) are experimental values, while the other curves are analytical results for each panel. The results for 0.8 A, 0.4 A, and 0 A are illustrated in green, red, and blue, respectively.

output different RDS shock signals, which will be applied to the EVS isolator. In this experiment, eight comparative tests are conducted with different shock intensities, as shown in Fig. 7. Detailed characteristics of the test shock signals are listed in Table V, such as rise time and the severity parameter β. The rise times of the shock inputs vary from 0.147 s to 0.055 s, corresponding to the severity parameter β increasing from 0.56 to 1.51.

By analyzing and summarizing the eight tests, the MAAR, MADR, and MRDR of the isolator are illustrated in Fig. 8 to further show the validity of the theoretical analysis and simulation. By observing Fig. 8(a), one can conclude that a greater current is preferable for reducing the acceleration response for both cases since the MAAR is the lowest when I = 0.8 A. This is due to the low-pass filtering effect introduced by a large positive current (negative EVS). That is to say, if the equivalent natural frequency of the system is low (a large positive current is applied), the system can act as a strong low-pass filter with large damping ratio, such that the effect of the shock is reduced. The displacement response is much more complicated. For the MADR shown in Fig. 8(b), both the simulation and experimental results show that passive system is superior to the EVS system when β is relatively small. The reason is that if a non-zero and positive current is applied, a negative VES is generated and reduces the overall stiffness of the system. Then, the displacement response becomes greater than that of the passive system because the system is softer in this case. As β increases, however, the nonlinearity becomes strong, and the nonlinear stiffness counteracts the effect of the negative VES, which leads to a higher overall stiffness and hence a smaller displacement response. Fig. 8(c) shows that the MRDR also depends on the current with a given amplitude and β. Since the MRDR represents the deformation of the isolator, it can be expected that a system with a lower overall stiffness may experience a larger deformation. However, this law is only obvious when β is relatively small. With an increase in β, systems with and without current begin to converge due to the nonlinearity caused by increasing β. Both the experiment and simulation have shown this trend.

In conclusion, the performance index should be decided first to choose appropriate isolator parameters which meet the requirements and provide better performance. From the point of view of reducing the acceleration response, it is beneficial to adopt a positive current (negative EVS). For limiting the deformation of the EVS isolator, a negative current (positive EVS) is preferable since it increases the anti-deformation ability of the system. The case of decreasing the absolute displacement response of the payload is conditional on the shock severity β, and a positive current is effective for most β values in minimizing the MADR.

D. Residual vibration suppression through bidirectional stiffness regulation

To further describe the appreciable benefits of the proposed EVS isolator, the strategies of stiffness regulation for shock isolation and residual vibration suppression are combined and tested in this section. As stated previously, regulating the stiffness is limited by certain conditions and purposes. Without loss of generality, we chose to focus on minimizing the acceleration response, $i.e.$, the MAAR, in this section. On one hand, acceleration-sensitive equipment is widely used in industry. On the other hand, the overresponse of the displacement caused by a shock input can be mitigated by some specific methods, such as adding a position limiting device. More concretely, we apply a positive current during the shock to decrease the acceleration response and adopt the extended strategy after the shock to shorten the settling time. It should be noted that when we say $during$ the shock, it denotes the time duration in which the payload oscillates from the initial position until it arrives at the steady position for the second time (see Fig. 3). This is because the maximum response usually occurs in this phase, so it is reasonable to implement the shock isolation strategy. After this period, attenuating the residual vibration isolation becomes the main focus, the residual vibration suppression strategy is then applied.

Since the RDS shock input is unknown in practice, and hence the steady position, it is impractical to judge the end of the shock by monitoring the position of the payload. However, the velocity of the payload reaches its maximal absolute value at steady position in a period. Besides, the velocity is easy to obtain through differentiating the position of the payload. Therefore, we use the velocity of the payload, instead of its position, to detect the end of the shock. Specifically, the moment when the velocity of the payload reaches the maximum

This article has been accepted for publication in a future issue of this journal, but has not been fully edited. Content may change prior to final publication. Citation information: DOI 10.1109/TMECH.2020.3029579, IEEE/ASME Transactions on Mechatronics

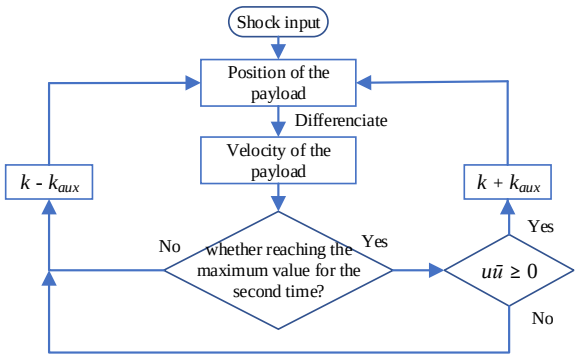

Fig. 9. Flow diagram for the combination of the strategies for shock isolation and residual vibration suppression.

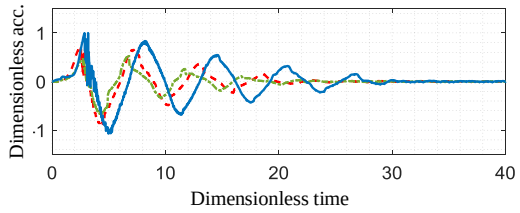

Fig. 10. Experimental acceleration response of the payload with the conventional strategy. Blue solid line: I = 0 A; red dashed line: I = 0.4 A; green dash-dotted line: I = 0.8 A.

absolute value for the second time is defined as the end of the shock. Before this moment, the strategy for shock isolation is activated; after this moment, the system soon turn to the strategy for residual vibration suppression. The corresponding flow diagram is shown in Fig. 9, which is programmed by the visual programming language LabVIEW. Firstly, the position of the payload is collected by a laser displacement sensor with a sampling rate of 1000 Hz. Secondly, the velocity is obtained by differentiating the collected displacement signal at the same sampling rate, and then applied as the basis of the bidirectional regulation of stiffness.

To reveal the advantages of the proposed extended strategy, both the conventional and extended strategies are tested and compared in the following. First of all, the conventional strategy cited and modified by Ref. [22–25] is tested with our

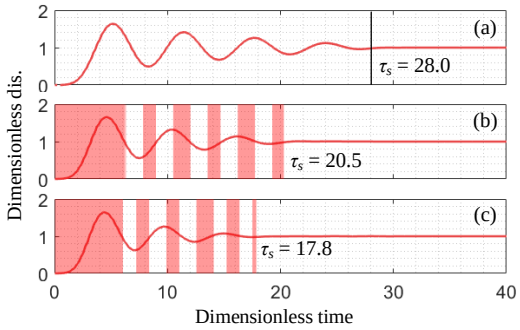

Fig. 11. Experimental displacement response of the mass with the conventional strategy. The pink and blank areas mean positive current is applied (-k_{aux} is added) and no current, respectively. (a) I = 0 A; (b) I = 0.4 A; (c) I = 0.8 A.

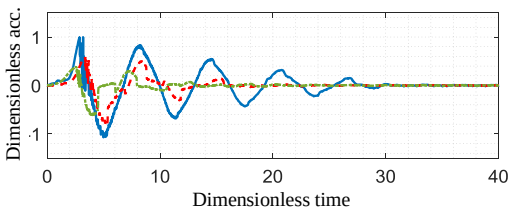

Fig. 12. Experimental acceleration response of the payload with the extended strategy. Blue solid line: I = 0 A; red dashed line: I = ± 0.4 A; green dash-dotted line: I = ± 0.8 A.

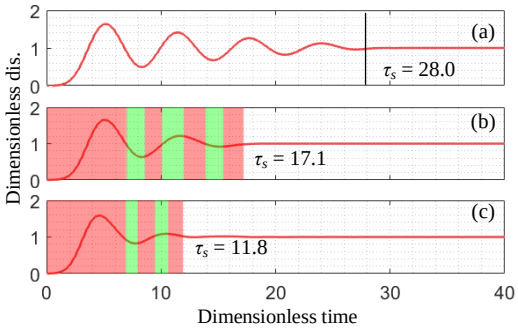

Fig. 13. Experimental displacement response of the mass with the extended strategy. The pink area corresponds to a positive current being applied (-k_{aux} is added), the green area corresponds to a negative current being applied (+k_{aux} is added), and the blank area corresponds to no current. (a) I = 0 A; (b) I = ± 0.4 A; (c) I = ± 0.8 A.

proposed prototype, and the results are shown in Fig. 10 and Fig. 11, in which the pink and blank areas mean a positive current I is applied (an auxiliary stiffness -k_{aux} is added) and no current (no auxiliary stiffness), respectively. It can be seen in Fig. 10 that the acceleration response is reduced during the shock, because the stiffness regulation strategy is adopted so the maximum acceleration response is suppressed. When the shock ends, the conventional strategy begins to take effect. With the increase in the current I, Δk increases; hence, the settling time τ_s decreases accordingly. Specifically, the results are 28.0 at 0 A, 20.5 at 0.4 A, and 17.8 at 0.8 A, as shown in Fig. 11. In conclusion, the conventional strategy can obtain decrease τ_s by 36.4% relative to that of a passive system.

For a comparison, the results of the extended strategy are shown in Fig. 12 and Fig. 13. Similarly, with the application of the extended strategy, the acceleration response illustrated in Fig. 12 is reduced during the shock as expected. Furthermore, the proposed extended strategy can achieve a shorter settling time τ_s than the conventional strategy, namely, 17.1 at 0.4 A and 11.8 at 0.8 A. This corresponds to a decrease of 57.9% compared to that of a passive system and a decrease of 33.7% compared to that of the system with the conventional strategy at I = 0.8 A. It should be pointed out that the alteration of stiffness varies frequencies of time responses. However, such frequency variation is relatively small since the stiffness of the system is repeatedly weakened and strengthened in a sequential way shown in Fig. 13.

VI. Conclusion

A novel VES isolator for shock isolation was designed and fabricated. The VES mechanism generates both negative and positive stiffnesses that can be superposed with the stiffness of the spring. In other words, the mechanism allows the overall stiffness of the system to increase and decrease by changing the magnitude and polarity of the exciting current, which results in bidirectional stiffness regulation and hence a wider range of stiffness variation. Based on this feature, a shock isolation strategy and an extended residual vibration suppression strategy are proposed. For shock isolation, the effect of the stiffness regulation strategy is tested by applying an RDS shock input to the base. For residual vibration suppression, both strategies are combined and tested. The experimental results reveal that the proposed isolator not only outperforms the passive isolator in terms of shock isolation but also outperforms the isolator with the conventional strategy in terms of residual vibration suppression.

References

[1] T. D. Le, M. T. N. Bui, and K. K. Ahn, "Improvement of vibration isolation performance of isolation system using negative stiffness structure," *IEEE/ASME Trans. Mechatron.*, vol. 21, no. 3, pp. 1561–1571, 2016.

[2] J. Ding, X. Luo, X. Chen, O. Bai, and B. Han, "Design of active controller for low-frequency vibration isolation considering noise levels of bandwidth-extended absolute velocity sensors," *IEEE/ASME Trans. Mechatronics*, vol. 23, no. 4, pp. 1832–1842, 2018.

[3] X. Sun and X. Jing, "A nonlinear vibration isolator achieving high-static-low-dynamic stiffness and tunable anti-resonance frequency band," *Mech. Syst. Signal Pr.*, vol. 80, pp. 166–188, 2016.

[4] Y. Zheng, X. Zhang, Y. Luo, Y. Zhang, and S. Xie, "Analytical study of a quasi-zero stiffness coupling using a torsion magnetic spring with negative stiffness," *Mech. Syst. Sig. Process.*, vol. 100, pp. 135–151, 2018.

[5] X. Liu, X. Huang, and H. Hua, "Performance of a zero stiffness isolator under shock excitations," *J. Vib. Control*, vol. 20, no. 14, pp. 2090–2099, 2013.

[6] B. Tang and M. J. Brennan, "On the shock performance of a nonlinear vibration isolator with high-static-low-dynamic-stiffness," *Int. J. Mech. Sci.*, vol. 81, no. 4, pp. 207–214, 2014.

[7] X. Huang, X. Liu, J. Sun, Z. Zhang, and H. Hua, "Vibration isolation characteristics of a nonlinear isolator using euler buckled beam as negative stiffness corrector: A theoretical and experimental study," *J. Sound Vib.*, vol. 333, no. 4, pp. 1132–1148, 2014.

[8] B. Yan, H. Ma, W. Zheng, B. Jian, K. Wang, and C. Wu, "Nonlinear electromagnetic shunt damping for nonlinear vibration isolators," *IEEE/ASME Trans. Mechatron.*, vol. 24, no. 4, pp. 1851–1860, 2019.

[9] N. Zhou and K. Liu, "A tunable high-staticlow-dynamic stiffness vibration isolator," *J. Sound Vib.*, vol. 329, no. 9, pp. 1254–1273, 2010.

[10] H. Pu, S. Yuan, Y. Peng, K. Meng, J. Zhao, R. Xie, Y. Huang, Y. Sun, Y. Yang, S. Xie, J. Luo, and X. Chen, "Multi-layer electromagnetic spring with tunable negative stiffness for semi-active vibration isolation," *Mech. Syst. Sig. Process.*, vol. 121, pp. 942–960, 2019.

[11] F. Zhang, S. Shao, Z. Tian, M. Xu, and S. Xie, "Active-passive hybrid vibration isolation with magnetic negative stiffness isolator based on maxwell normal stress," *Mech. Syst. Sig. Process.*, vol. 123, pp. 244–263, 2019.

[12] J. Zhou, Q. Xiao, D. Xu, H. Ouyang, and Y. Li, "A novel quasi-zero-stiffness strut and its applications in six-degree-of-freedom vibration isolation platform," *J. Sound Vib.*, vol. 394, pp. 59–74, 2017.

[13] M. Sun, G. Song, Y. Li, and Z. Huang, "Effect of negative stiffness mechanism in a vibration isolator with asymmetric and high-static-low-dynamic stiffness," *Mech. Syst. Sig. Process.*, vol. 124, pp. 388–407, 2019.

[14] G. Dong, X. Zhang, S. Xie, B. Yan, and Y. Luo, "Simulated and experimental studies on a high-static-low-dynamic stiffness isolator using magnetic negative stiffness spring," *Mech. Syst. Sig. Process.*, vol. 86, pp. 188–203, 2017.

[15] A. Carrella, M. J. Brennan, T. P. Waters, and V. L. Jr, "Force and displacement transmissibility of a nonlinear isolator with high-static-low-dynamic-stiffness," *Int. J. Mech. Sci.*, vol. 55, no. 1, pp. 22–29, 2012.

[16] C. Cheng, S. Li, Y. Wang, and X. Jiang, "Force and displacement transmissibility of a quasi-zero stiffness vibration isolator with geometric nonlinear damping," *Nonlinear Dyn.*, vol. 87, no. 4, pp. 1–13, 2016.

[17] X. Huang, X. Liu, and H. Hua, "Effects of stiffness and load imperfection on the isolation performance of a high-static-low-dynamic-stiffness non-linear isolator under base displacement excitation," *Int. J. Nonlin. Mech.*, vol. 65, no. 1, pp. 32–43, 2014.

[18] H. Ding, Z. Lu, and L. Chen, "Nonlinear isolation of transverse vibration of pre-pressure beams," *J. Sound Vib.*, vol. 442, pp. 738–751, 2019.

[19] D. Ning, H. Du, S. Sun, W. Li, N. Zhang, and M. Dong, "A novel electrical variable stiffness device for vehicle seat suspension control with mismatched disturbance compensation," *IEEE/ASME Trans. Mechatron.*, vol. 24, no. 5, 2019.

[20] X. Huang, Y. Chen, H. Hua, X. Liu, and Z. Zhang, "Shock isolation performance of a nonlinear isolator using euler buckled beam as negative stiffness corrector: Theoretical and experimental study," *J. Sound Vib.*, vol. 345, no. 4, pp. 178–196, 2015.

[21] A. Ramaratnam and N. Jalili, "A switched stiffness approach for structural vibration control: theory and real-time implementation," *J. Sound Vib.*, vol. 291, no. 1, pp. 258–274, 2006.

[22] J. Onoda, T. Endot, H. Tamaoki, and N. Watanabe, "Vibration suppression by variable-stiffness members," *AIAA J.*, vol. 29, no. 6, pp. 977–983, 1991.

[23] J. Onoda, T. Sano, and K. Kamiyama, "Active, passive, and semiactive vibration suppression by stiffness variation," *AIAA J.*, vol. 30, no. 30, pp. 2922–2929, 1992.

[24] D. F. Ledezma-Ramirez, N. S. Ferguson, and M. J. Brennan, "Shock isolation using an isolator with switchable stiffness," *J. Sound Vib.*, vol. 330, no. 5, pp. 868–882, 2011.

[25] ——, "An experimental switchable stiffness device for shock isolation," *J. Sound Vib.*, vol. 331, no. 23, pp. 4987–5001, 2012.

[26] D. F. Ledezma-Ramirez, J. J. Villalobos-Luna, N. S. Ferguson, and M. J. Brennan, "Theoretical and experimental analysis of shock isolation using non linear stiffness." *J. Acoust. Soc. Am.*, vol. 134, no. 5, pp. 4197–4197, 2013.

[27] J. Chen, "Response of large space structures with stiffness control," *J. Spacecraft Rockets*, vol. 21, no. 5, pp. 463–467, 1984.

[28] Y. Sun, J. Zhao, M. Wang, Y. Sun, H. Pu, J. Luo, Y. Peng, S. Xie, and Y. Yang, "High-static-low-dynamic stiffness isolator with tunable electromagnetic mechanism," *IEEE/ASME Transactions on Mechatronics*, vol. 25, pp. 316–326, 2019.

[29] W. Robertson, B. Cazzolato, and A. Zander, "Axial force between a thick coil and a cylindrical permanent magnet: Optimising the geometry of an electromagnetic actuator," *IEEE Trans. Magn.*, vol. 48, no. 9, pp. 2479–2487, 2012.

[30] A. Shiri and A. Shoulaie, "A new methodology for magnetic force calculations between planar spiral coils," *Prog. Electromag. Res.*, vol. 95, pp. 39–57, 2009.

[31] Y. Sun, K. Meng, S. Yuan, J. Zhao, R. Xie, Y. Yang, J. Luo, Y. Peng, S. Xie, and H. Pu, "Modeling electromagnetic force and axial-stiffness for an electromagnetic negative-stiffness spring toward vibration isolation," *IEEE Trans. Magn.*, vol. 55, no. 3, pp. 1–10, 2019.

[32] N. C. Shekhar, H. Hatwal, and A. K. Mallik, "Response of non-linear dissipative shock isolators," *J. Sound Vib.*, vol. 214, no. 4, pp. 589–603, 1998.

[33] T. Tran and K. Liu, "Time-delay control of a switchable stiffness system," *J. Vib. Control*, vol. 23, no. 15, pp. 2375–2390, 2015.

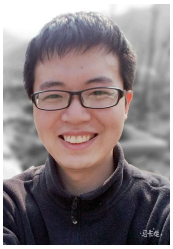

Jinglei Zhao received B.Eng., M.Sc and Ph.D. degrees in Mechanical Engineering from Shanghai University (Shanghai, China) in 2012, 2015 and 2020, respectively. He is currently a postdoctoral researcher in the State Key Laboratory of Mechanical Transmissions and College of Mechanical engineering, Chongqing University (Chongqing, China). His research interests include modeling of nonlinear vibration isolation systems.

Yi Sun received his B.Eng degrees in Mechanical Engineering in 2003, and M.Eng degree in Mechatronic Engineering in 2006, all from Huazhong University of Science and Technology (Wuhan, China). In 2013, he received his Dr.Eng degree in Robotics from Ritsumeikan University (Kyoto, Japan). In July 2016, granted by the Program of Young Eastern Scholar of Shanghai, he joined Shanghai University as an Assistant Professor. His research interests include robotics and vibration controlling.

Jiheng Ding received the B.E. degree in automation from Chongqing University, Chongqing, China, in 2007, the M.E. degree in control theory and control engineering from Xi'an University of Architecture and Technology, Shaanxi, China, in 2011, and the Ph.D. degree at the School of Mechanical Science and Engineering, Huazhong University of Science and Technology, Wuhan, China. He has been a lecturer at Shanghai University(Shanghai, China) since 2019. His research interests include control of electromechanical systems and active vibration isolation.

Yu Sun received the B.S. degree in electrical engineering from Dalian University of Technology, Dalian, China, in 1996, the M.S. degree from the Institute of Automation, Chinese Academy of Sciences, Beijing, China, in 1999, and the M.S. degree in electrical engineering and the Ph.D. degree in mechanical engineering from the University of Minnesota, Minneapolis, MN, USA, in 2001 and 2003, respectively. He is a Professor with the Department of Mechanical and Industrial Engineering, University of Toronto, Toronto, ON, Canada. His research areas include the design and fabrication of M/NEMS devices, micronanorobotic manipulation, and the manipulation and characterization of cells, biomolecules, and nanomaterials.

Min Wang received his B.Eng and M.Eng degree in Mechatronic Engineering in 2012 from Wuhan University of Technology (Wuhan, China) in School of Mechanical and Electronic Engineering. In 2018, he received his Dr.Eng degree in Vibration Isolation and Active Control from Huazhong University of Science and Technology (Wuhan, China). He is now working as a lecturer in Shanghai University, and his research interests include vibration isolation and controlling.

Shujin Yuan received his B.Eng. degree in Mechanical Engineering and Automation from Shanghai University (Shanghai, China) in 2016, and then continued to study for Dr. Eng. degree in Mechanical Engineering at Shanghai University. His research interests include vibration and noise control, and mechanical systems.

This article has been accepted for publication in a future issue of this journal, but has not been fully edited. Content may change prior to final publication. Citation information: DOI 10.1109/TMECH.2020.3029579, IEEE/ASME Transactions on Mechatronics

Huayan Pu received the M.Sc. and Ph.D. degrees in mechatronics engineering from Huazhong University of Science and Technology (Wuhan, China) in 2007 and 2011, respectively. Currently, she is a Professor at Shanghai University (Shanghai, China). Her current research interests include vibration controlling and robotics. Dr. Pu was awarded the best paper in biomimetics at the 2013 IEEE International Conference on Robotics and Biomimetics. She was also nominated as the best conference paper finalist at the 2012 IEEE International Conference on Robotics and Biomimetics.

Jun Luo received the B.S. and M.S. degrees in mechanical engineering from Henan Polytechnic University (Jiaozuo, China) in 1994 and 1997, respectively, and the Ph.D. degree from the Research Institute of Robotics, Shanghai Jiao Tong University (Shanghai, China) in 2000. He is a Professor in the State Key Laboratory of Mechanical Transmissions, Chongqing University (Chongqing, China). His research areas include robot sensing, man-machine interfaces, and special robotics.

Zhijiang Xie received the B.S. degree in mechanical engineering from Henan Polytechnic University (Jiaozuo, China) in 1983, and the M.S. and Ph.D. degrees in mechanical engineering from Chongqing University (Chongqing, China) in 1992 and 1996, respectively. He is a Professor in the State Key Laboratory of Mechanical Transmissions, Chongqing University (Chongqing, China). His research areas include equipment monitoring and control.

Yi Qin received the B.S. degree in mechanical engineering and the Ph.D. degree in mechatronics engineering from Chongqing University (Chongqing, China) in 2004 and 2008, respectively. He is a Professor in the State Key Laboratory of Mechanical Transmissions, Chongqing University. His research areas include intelligent fault diagnosis and prediction.

Jing Wei received the B.S. degree in mechanical engineering from Chongqing University of Technology (Chongqing, China) in 2000, the M.S. degree in mechanical engineering from Xihua University (Sichuan, China) in 2005, and the Ph.D. degree in mechanical engineering in Chongqing University (Chongqing, China), respectively. He is a Professor in the State Key Laboratory of Mechanical Transmissions, Chongqing University. His research areas include mechanical transmission design.

Shaorong Xie received the B. Eng. and M. Eng. degrees in mechanical engineering from Tianjin Polytechnic University (Tianjin, China) in 1995 and 1998, respectively, and the Ph.D. Eng. degree in mechanical engineering from the Institute of Intelligent Machines at Tianjin University and the Institute of Robotics and Automatic Information System, Nankai University (Tianjin, China) in 2001. She is a Professor with the School of Mechatronic Engineering and Automation, Shanghai University (Shanghai, China). Her research areas include advanced robotics technologies and bionic control mechanisms.

Yan Peng received the Ph.D. degree in pattern recognition and intelligent systems from Shenyang Institute of Automation, Chinese Academy of Sciences (Shenyang, China) in 2009. She is currently a Professor with Shanghai University (Shanghai, China) where she is the Executive Dean of the Research Institute of USV Engineering. Her current research interests include modeling and control of unmanned surface vehicles, field robotics, and locomotion systems.